Configurable error correction of code-division multiplexed TES detectors with a cryotron switch

Joel C. Weber, Joseph W. Fowler, Malcolm Durkin, Kelsey M. Morgan (iD), John A. B. Mates, Doug A. Bennett (iD), W. Bertrand Doriese, Daniel R. Schmidt, Gene C. Hilton, Daniel S. Swetz (iD), and Joel N. Ullom

View Online   Export Citation   CrossMark

ARTICLES YOU MAY BE INTERESTED IN

Configurable error correction of code-division multiplexed TES detectors with a cryotron switch

View Online

Export Citation

CrossMark

Joel C. Weber,[1,2,a] Joseph W. Fowler,[1,2] Malcolm Durkin,[1,2] Kelsey M. Morgan,[1,2] John A. B. Mates,[1,2]
Doug A. Bennett,[1] W. Bertrand Doriese,[1] Daniel R. Schmidt,[1] Gene C. Hilton,[1] Daniel S. Swetz,[1]
and Joel N. Ullom[1,2]

AFFILIATIONS

[1]National Institute of Standards and Technology, Boulder, Colorado 80305, USA
[2]Department of Physics, University of Colorado, Boulder, Colorado 80309, USA

[a]Author to whom correspondence should be addressed: joel.weber@colorado.edu

ABSTRACT

The development of a superconducting analog to the transistor with extremely low power dissipation will accelerate the proliferation of low-temperature circuitry operating in the milliKelvin regime. The thin-film, magnetically actuated cryotron switch is a candidate building block for more complicated and flexible milliKelvin circuitry. We demonstrate its utility for implementing reconfigurable circuitry by integrating a cryotron switch into flux-summed code-division SQUID multiplexed readout for large arrays of transition-edge-sensor (TES) microcalorimeters. Code-division multiplexing eliminates the noise penalty of time-division multiplexing while being drop-in compatible with the latter's control electronics. However, code-division multiplexing is susceptible to single-point failure mechanisms which can result in an unconstrained demodulation matrix and the loss of information from many sensing elements. In the event of a failure, the integrated cryotron switch provides a zero-signal output from a single TES, enabling the demodulation matrix used to compute TES signals from SQUID signals to be constrained and data recovered from the remaining sensors. This demonstration of configurable error correction provides both a real-world application of the cryotron switch and a foundation for more complex circuitry at milliKelvin temperatures.

https://doi.org/10.1063/1.5089870

A transistor is a quintessential three-terminal device in which a control signal applied to one terminal modulates electrical transport between the other two. The modern semiconductor-electronics industry is based on the hierarchical organization of transistors into logic gates and then functional units such as processors. There has been a lengthy search for a comparable three-terminal device that is compatible with superconducting electronics and cryogenic temperatures.[1–5] Superconducting electronics are under consideration for applications in classical computing,[6] quantum computing,[7] and sensing.[8–11] A three-terminal device would create possibilities for logic, amplification, and interfaces between different circuit elements. The "nanocryotron" shows considerable potential in this regard.[12–14] In this device, the control terminal is galvanically joined to a superconducting nanowire and the control current creates a resistive hotspot that modulates the channel conductance. The steady-state power in an actuated nanocryotron is at least several nanowatts,[12] a level that is acceptable in the few-Kelvin regime but limiting at the milliKelvin temperatures required for many superconducting sensors where the cooling power available for the entire payload might be 1 μW or less.

To create a switching element suitable for milliKelvin applications, we previously re-introduced the "magnetically actuated cryotron."[15] This device is a miniaturized, thin-film implementation of the bulk superconducting switch developed by Buck in the 1950s.[16] In the magnetically actuated cryotron, a magnetic field induced by current in the control line suppresses superconductivity in the signal wire. A fourth terminal allows the control functionality of the magnetically actuated cryotron to be galvanically isolated from the signal channel.

In this letter, we show how the use of the magnetically actuated cryotron enables complex functionality in a circuit at milliKelvin temperatures. Traditionally, milliKelvin circuitry is literally and functionally frozen; it can only be modified to adapt to changing circumstances via warming to room temperature for rework. In contrast, the use of the cryotron as a low-temperature switch allows a sensing circuit to be reconfigured while cold to recover from a hardware fault that would ordinarily result in a substantial loss of capability. The substrate area, power, and control wiring required for the cryotron are negligible. Our results suggest that the cryotron can provide dynamic configurability and other sophisticated functionalities which are already common in semiconductors to cryogenic circuitry.

Our development of the magnetically actuated cryotron is partly driven by demands for readout of increasingly large transition-edge-sensor (TES) arrays for applications in materials science and astrophysics. TESs provide high collecting efficiencies and state-of-the-art resolving powers for single x-ray photons.[8,17,18] Existing arrays contain hundreds of detectors,[9] but future systems aim to push this number to 10^4–10^5 pixels.[19,20] A variety of multiplexing strategies are in development.[21–26]

Flux-summed code-division multiplexing (ϕ-CDM) is a promising candidate for multiplexing large arrays.[27] In CDM, N TESs, where N is a multiple of 4, are encoded with a $N \times N$ Hadamard code (see Appendix A in the supplementary material).[28,29] In a Hadamard code, each row consists of N elements with values of $+1$ or -1; the N rows are orthogonal. The N TES signals are summed into N readout superconducting quantum interference device (SQUID) amplifiers via lithographically patterned inductive coils. ϕ-CDM is drop-in compatible with existing time-division multiplexing (TDM) electronics, wherein row activation resources are shared among different columns. We discuss the sequential readout of a single SQUID column in this application, but all results shown here are readily scalable to multiple readout columns.[22] Because the signal from the N dc-biased TESs is present in each SQUID measurement and SQUID-amplifier noise is added incoherently during demodulation, the $\sqrt{N}$ noise penalty inherent to TDM is avoided in CDM. To reconstruct photon events, data from N successive SQUID measurements are multiplied by the inverse of the Hadamard code. We have demonstrated 32-row ϕ-CDM readout (CDM-32) with a resolution of 2.77 ± 0.02 eV FWHM at 5.9 keV.[30]

A potential limitation of CDM is that data from all SQUIDs in a column are necessary to decode the TES signal. If a single SQUID fails, for example, due to static discharge or radiation damage, the demodulation process becomes under-constrained and information from the entire column of TESs is lost.[22] As the CDM multiplexing factor is expanded to 64 and beyond, the small probability of certain failure modes disabling many TESs becomes unacceptable, particularly in the case of satellite missions where servicing the payload is not an option. It has been demonstrated that TES signals can be recovered through error correction (EC) in the event of a SQUID failure if one TES is replaced with a constant signal.[31] This can be achieved with an over-constrained Hadamard code with more SQUIDs than TESs present. However, in ϕ-CDM, where the Hadamard code is defined through lithographic traces, this practice is wasteful and space-consuming in the absence of a failure event (in CDM-16, 1/16 of the multiplexing factor would be lost). To address this, we introduce configurable error correction (CEC) through implementation of a superconducting switch, whereby a TES channel is disabled for EC only when needed (Fig. 1). A cryotron switch was selected for this application instead of an electrothermal or a tunnel-junction switch due to its low power dissipation, low activation current, high signal-current capacity, and galvanic isolation of the signal from control.[16] Furthermore, the small size of the cryotron switch used allows it to be easily integrated with a CDM circuit and occupies a $20\times$ less area than an over-constrained Hadamard EC scheme.

The cryotron switch used here for CEC is modified from the thin-film design described by Lowell et al.[15] The magnetic field created by current passing in the control line drives the signal line normal (effectively, open). A superconducting transformer provides a $10\times$ increase in effective control current; its dipole-gradiometric
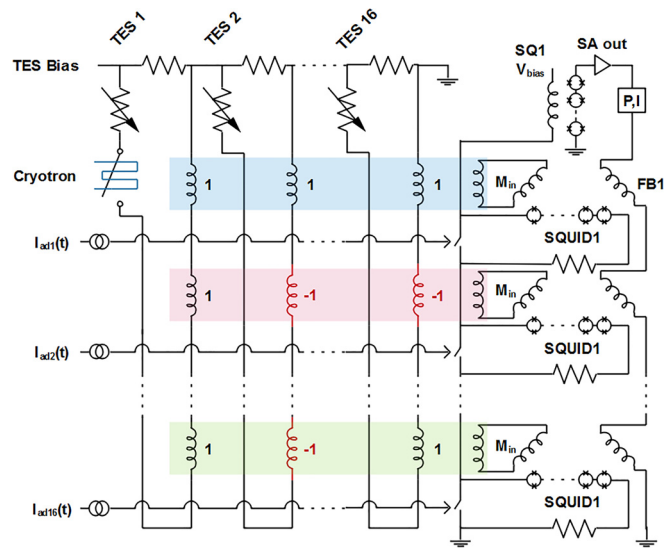

FIG. 1. Circuit diagram of a 16-channel ϕ-CDM circuit with a cryotron switch for CEC. In the physical layout of the circuit, TES pixels are wire bonded to interface (IF) chips (with shunt resistors and Nyquist inductors for optimizing x-ray readout) which are in turn wire bonded to a CDM SQUID chip for multiplexing.[32] The control current changes the cryotron signal line to normal (open-state), eliminating the signal from TES 1. The Hadamard code associated with each TES signal is defined lithographically via the winding direction of the coil summing into the mutual inductance, M_{in}. The readout SQUIDs are run as a conventional TDM and addressed via flux-actuated switching.[33]

design reduces sensitivity to external magnetic fields. This cryotron is integrated into our standard interface (IF) chip fabrication[21] with the addition of an AlMn layer for the signal line and a Nb layer for cross-over wiring (Fig. 2). To create a large open-state resistance, the Nb
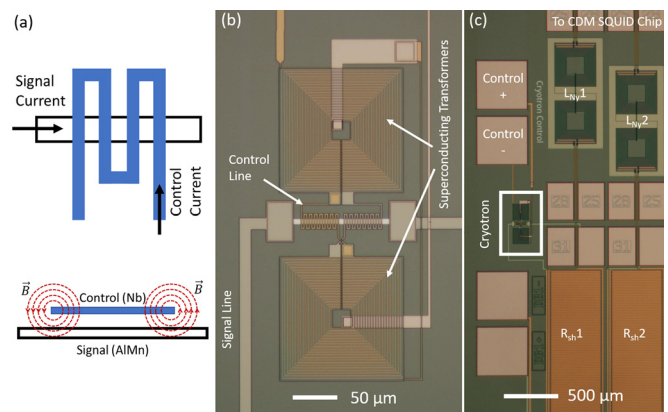

FIG. 2. (a) Schematic of cryotron switch and operation. An AlMn signal line is switched from superconducting to normal via the magnetic fields ($\vec{B}$) generated by current at the edges of the winding Nb control line.[15] (b) Detailed view of the cryotron with the superconducting transformers in a dipole gradiometer orientation. (c) The first 2 channels of a 32-channel "interface chip" (IF). In our implementation of CDM, the TES shunt resistors (R_{sh}) and bandwidth-limiting inductors (L_{Ny}) for a readout column are deposited on the IF. The cryotron signal line is in series with TES 1, while the "control" bond pads are used to activate the cryotron.

control line is meandered across the signal line so that a more extended length of the signal line can be driven normal. The cryotron geometry used here has an open-state resistance of 10 Ω in the limit of zero signal current. When the switch is closed, the signal line has a critical current of ∼350 μA, which exceeds requirements during TES operation and diagnostic sweeps of the TES *I-V* curves. The labeled bond pads in Fig. 2(c) on the IF chip from our standard TDM/CDM electronics provide the control-line signal of ∼2 mA. When the switch is opened, current is redirected from the highly resistive TES arm of the bias circuit into the parallel bias resistor, the TES enters its super-conducting state, and there is a constant, near zero signal from this TES channel into the SQUIDs of the multiplexer column.

To test the efficacy of CEC, we wired our IF chip to the 32-row φ-CDM chip used by Morgan *et al.*[30] To simplify analysis, we only wire bonded the first 16 rows. We also used the same TES array as Morgan, which consisted of 350 μm × 350 μm Mo/Cu bilayers with 2.5 μm thick bismuth for added absorption.[32] We measured the Mn Kα (5.9 keV) fluorescence spectrum first with the cryotron in its closed state to confirm that its presence had no effect on the IF chip. With ∼10 000 x-rays per TES (at a count rate of ∼1 x-ray per TES per second), a combined spectrum of data from 15 of the 16 TESs achieved a resolution of 2.96 ± 0.03 eV [Fig. 3(a)], comparable to pre-viously published results. Resolution data from TES 1 were excluded from the average to ensure consistency between measurements with the cryotron in an open and closed state. We next supplied a control current of 2 mA to the cryotron to disable TES 1 and again recorded ∼10 000 x-rays per TES. Here, we achieved a resolution of 2.91 ± 0.03 eV [Fig. 3(b)], consistent with the previous result. Demodulated data showed no x-rays recorded by TES 1, demonstrat-ing switching during operation.
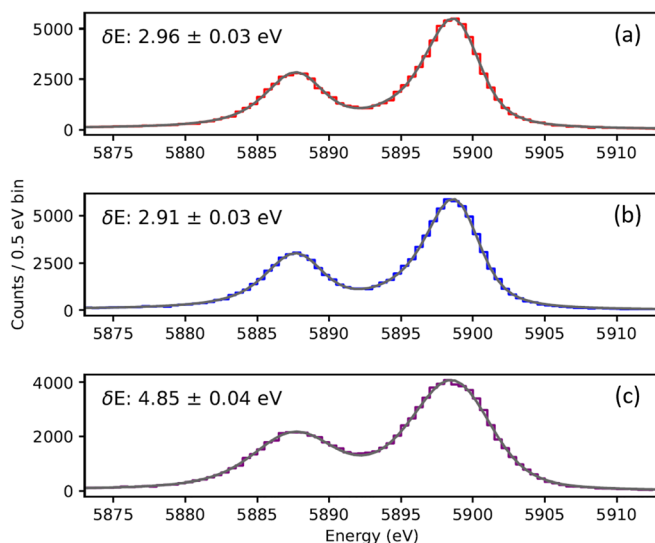
To simulate a SQUID failure event, we can omit measurements from any one of the SQUID channels and use the zero-signal from the TES circuit with the switched cryotron to constrain our demodulation matrix. We removed the SQUID 11 data from the output vector and demodulated the raw signal with a 15 × 15 inversion matrix, enabling recovery of measured x-ray pulses, shown in Fig. 3(c). It is seen that the achieved resolution with CEC has increased to 4.85 ± 0.04 eV (the resolution for all 16 simulated SQUID failures is shown in Appendix A in the supplementary material) which is attributed to a combination of two factors. The first effect is smaller and arises from demodulating a 15 × 15 matrix. When the Hadamard code is $N \times N$ where N is a multiple of 4, the inversion matrix contains a nonzero value for each matrix index. Practically, this means that TES information is contained in each SQUID and each time step during data recording. When the matrix no longer meets this size criterion, a percentage of the inversion matrix values becomes 0 (47% for a 15 × 15 case), meaning that TES information is lost during various time intervals resulting in more ali-asing of readout noise into the signal bandwidth.[31] This effect can be modeled for the existing circuit's shunt-resistor and Nyquist-inductor values and is shown to produce a 9% or 0.25 eV degradation in the final resolution. This value can be improved by adjusting Nyquist inductance and shunt resistance parameters to deemphasize readout noise relative to TES noise.

The second and dominant source of noise is a low-frequency component generated by operation of the cryotron [Fig. 4]. In an ideal demonstration of CEC, the TES switched off by the cryotron has a constant signal output with no noise. This assumption enables us to constrain the demodulation matrix in the event of a SQUID failure. However, if this assumption is incorrect and the disabled TES pro-duced noise or spurious signals that are not accounted for during demodulation, then this low-frequency component will be added to the other, active TES detectors and worsen their energy resolution. While the source of the low-frequency noise shown in Fig. 4 is not fully understood, it is believed to be caused by an unwanted thermal component in the activation of the cryotron (e.g., a varying resistance in the signal line).

To verify that the noise in the switched TES channel is responsi-ble for the observed resolution degradation, we performed various signal-to-noise calculations. The customary way to predict the energy resolution is to measure an average pulse response to x-rays and noise in the absence of pulses and from these measurements integrate the signal-to-noise ratio over frequency.[34] However, this approach pre-dicted a resolution of ∼1 eV worse than the achieved results for both the CDM-16 and CDM-15 cases. While this offset is not fully under-stood, our best explanation is to attribute it to nonstationary behavior in the TES, wherein its noise is suppressed at the higher resistance val-ues encountered at the peak of a pulse, enabling a better resolution than that explained by the quiescent noise.[35] As an alternative estima-tion approach, we examined the ratio of achieved resolution between CDM-16 and CDM-15 and compared it to the ratio of the predicted resolution of CDM-16 to CDM-15 based on both noise records (with-out x-ray pulses) and the root-mean-square (rms) noise levels observed during the pretrigger period of pulse records. We found that the ratio of achieved resolutions closely tracked the ratio of predicted resolutions: the ratios agreed to 15% (2%) when the quiescent noise (pretrigger rms) was used for the predictions. Hence, the low-frequency noise observed in the cryotron-switched channel is

FIG. 3. Mn Kα x-ray fluorescence spectra from φ-CDM. (a) CDM-16 has a mea-sured energy resolution of 2.96 ± 0.03 eV with the cryotron in a closed state (all 16 SQUIDs and TESs working normally). (b) CDM-16 has a measured energy resolu-tion of 2.91 ± 0.03 eV with the cryotron in an open state (16 SQUIDs, 15 TESs enabled). (c) CDM-15 demonstration of CEC with a simulated SQUID 11 failure yields an energy resolution of 4.85 ± 0.04 eV (15 SQUIDs, 15 TESs enabled).
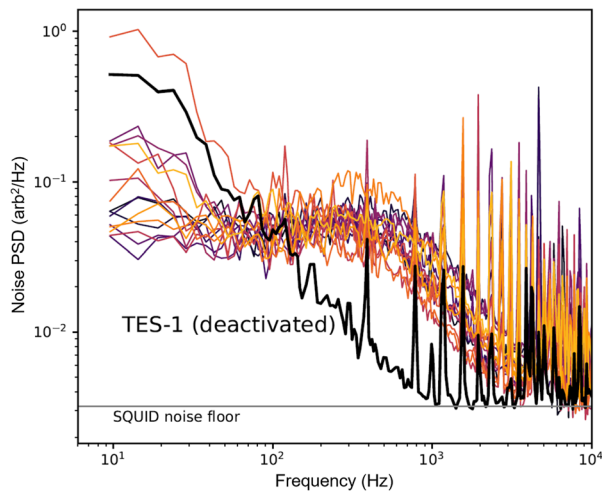
FIG. 4. Noise profile for all 16 TESs for the dataset with the cryotron activated (TES 1 disabled). The black curve shows the measurement from the channel whose TES is disabled, while the remaining curves show measurements from the 15 active TES channels. Low-frequency noise in the disabled channel above the indicated SQUID noise floor causes a degradation in the resolution in the other TES channels when CEC is employed. Above average low-frequency noise is also seen in one of the activated channels but does not adversely affect the resolution during CEC. The lines above 2 kHz are electrical interference and have almost no effect on the sensor resolution because they are outside the TES's signal band.

sufficient to explain the discrepancy between the 4.85 eV resolution observed in CDM-15 and the ∼3.25 eV resolution expected after accounting for the zero-value entries in the inversion matrix.

In a future implementation of CEC, we would seek to eliminate or minimize the low-frequency noise observed in this demonstration. Possible avenues would be to increase the open-state resistance of the cryotron or to remove any thermal components to switching. The first option is to increase the length of the signal line and the number of control line crossings to increase the surface area penetrated by magnetic fields. Using this technique, we have demonstrated a switch with an open-state resistance of 50 Ω. This value could be pushed higher if needed by applications with low leakage-current requirements. The second option is to increase the control current available for cryotron switching via an increase in the superconducting transformer size or a decrease in the Nb-coil pitch through electron beam lithography to allow more windings and greater current gain through the transformer. As the maximum magnetic field seen by the signal line is proportional to the control current, a higher available control current will more readily activate magnetic switching.

Even without these design changes, it is possible to achieve a much better resolution from CEC when photon rates are low. When the cryotron deactivates TES 1, the demodulation described so far ensures that exactly one active TES contributes to each demodulated signal channel. This zero-mixing requirement is essential when photon rates are high enough that multiple events are expected within a readout column during a pulse record length. At low photon rates, however, it unnecessarily constrains the possible demodulations. In Appendix B (supplementary material), we discuss an alternative approach, noise-optimal demodulation, which reduces the overall noise level in the demodulated signals at the price of elevated crosstalk

between channels. Noise-optimal demodulation produces a resolution of 3.18 ± 0.04 eV in our CDM-15 case.

In summary, we have demonstrated configurable error correction for code-division multiplexing of TES x-ray microcalorimeters. We integrated a thin-film cryotron switch into the TES bias circuitry and acquired x-ray-pulse data. When the cryotron was superconducting (closed), the spectral resolution of the 16 TESs in the readout column was comparable to earlier experiments in which there was no cryotron. When the cryotron was normal (open), it disabled one TES in the readout column and the resolution of the other TESs was unaffected. Finally, we simulated a SQUID failure that would otherwise result in loss of information from all TESs in the column. We recovered data from the 15 remaining TESs by making use of the known (constant) signal from the disabled TES. This demonstration provides a way to mitigate the risk to a readout column from a first-stage SQUID failure in code-division multiplexing. This demonstration also establishes the feasibility of reconfigurable circuitry in the milliKelvin regime which is a capability that is expected to have applications in cryogenic electronics beyond sensor readout. For example, cryotron-based switch networks may one day route control signals in superconducting classical or quantum computing architectures.

See the supplementary material for a detailed breakdown of the linear algebra used for the modulation and demodulation of both standard CDM and CEC. It also includes a description of noise-optimal demodulation, an alternative to CEC when low x-ray counting rates minimize crosstalk.

REFERENCES

[1]K. E. Gray, "A superconducting transistor," Appl. Phys. Lett. **32**(6), 392–395 (1978).

[2]S. Faris, S. Raider, W. Gallagher, and R. Drake, "Quiteron," IEEE Trans. Magn. **19**(3), 1293–1295 (1983).

[3]A. Morpurgo, T. Klapwijk, and B. Van Wees, "Hot electron tunable supercurrent," Appl. Phys. Lett. **72**(8), 966–968 (1998).

[4]N. E. Booth, P. A. Fisher, M. Nahum, and J. N. Ullom, "A superconducting transistor based on quasiparticle trapping," Supercond. Sci. Technol. **12**(8), 538 (1999).

[5]S.-B. Lee, G. D. Hutchinson, D. A. Williams, D. G. Hasko, and H. Ahmed, "Superconducting nanotransistor based digital logic gates," Nanotechnology **14**(2), 188 (2003).

[6]D. S. Holmes, A. L. Ripple, and M. A. Manheimer, "Energy-efficient superconducting computing—Power budgets and requirements," IEEE Trans. Appl. Supercond. **23**(3), 1701610–1701610 (2013).

[7]G. Wendin, "Quantum information processing with superconducting circuits: A review," Rep. Prog. Phys. **80**(10), 106001 (2017).

[8]K. D. Irwin and G. C. Hilton, "Transition-edge sensors," in *Cryogenic Particle Detection* (Springer, 2005), pp. 63–150.

[9]J. N. Ullom and D. A. Bennett, "Review of superconducting transition-edge sensors for X-ray and gamma-ray spectroscopy," Supercond. Sci. Technol. **28**(8), 084003 (2015).

[10]G. C. O'Neil, L. Miaja-Avila, Y. I. Joe, B. K. Alpert, M. Balasubramanian, D. Sagar, W. Doriese, J. W. Fowler, W. K. Fullagar, and N. Chen, "Ultrafast time-resolved X-ray absorption spectroscopy of ferrioxalate photolysis with a laser plasma X-ray source and microcalorimeter array," J. Phys. Chem. Lett. **8**(5), 1099–1104 (2017).

[11]L. Miaja-Avila, G. C. O'Neil, Y. I. Joe, B. K. Alpert, N. H. Damrauer, W. B. Doriese, S. M. Fatur, J. W. Fowler, G. C. Hilton, and R. Jimenez, "Ultrafast

time-resolved hard X-ray emission spectroscopy on a tabletop," Phys. Rev. X **6**(3), 031047 (2016).

[12]A. N. McCaughan and K. K. Berggren, "A superconducting-nanowire three-terminal electrothermal device," Nano Lett. **14**(10), 5748–5753 (2014).

[13]Q.-Y. Zhao, E. A. Toomey, B. A. Butters, A. N. McCaughan, A. E. Dane, S.-W. Nam, and K. K. Berggren, "A compact superconducting nanowire memory element operated by nanowire cryotrons," Supercond. Sci. Technol. **31**(3), 035009 (2018).

[14]Q.-Y. Zhao, A. N. McCaughan, A. E. Dane, K. K. Berggren, and T. Ortlepp, "A nanocryotron comparator can connect single-flux-quantum circuits to conventional electronics," Supercond. Sci. Technol. **30**(4), 044002 (2017).

[15]P. J. Lowell, J. A. Mates, W. B. Doriese, G. C. Hilton, K. M. Morgan, D. S. Swetz, J. N. Ullom, and D. R. Schmidt, "A thin-film cryotron suitable for use as an ultra-low-temperature switch," Appl. Phys. Lett. **109**(14), 142601 (2016).

[16]D. A. Buck, "The cryotron-a superconductive computer component," Proc. IRE **44**(4), 482–493 (1956).

[17]C. A. Kilbourne, W. B. Doriese, S. R. Bandler, R. P. Brekosky, A.-D. Brown, J. A. Chervenak, M. E. Eckart, F. M. Finkbeiner, G. C. Hilton, and K. D. Irwin, "Multiplexed readout of uniform arrays of TES x-ray microcalorimeters suitable for Constellation-X," in *Space Telescopes and Instrumentation 2008: Ultraviolet to Gamma Ray* (International Society for Optics and Photonics, 2008).

[18]J. Uhlig, "Life of a photon in X-ray spectroscopy," Ph.D. thesis (Lund University, Lund, Sweden, 2011).

[19]L. Ravera, D. Barret, J. W. den Herder, L. Piro, R. Clédassou, E. Pointecouteau, P. Peille, F. Pajot, M. Arnaud, and C. Pigot, "The X-ray integral field unit (X-IFU) for Athena," in *Space Telescopes and Instrumentation 2014: Ultraviolet to Gamma Ray* (International Society for Optics and Photonics, 2014).

[20]J. A. Gaskin, M. C. Weisskopf, A. Vikhlinin, H. D. Tananbaum, S. R. Bandler, M. W. Bautz, D. N. Burrows, A. D. Falcone, F. A. Harrison, and R. K. Heilmann, "The X-ray surveyor mission: A concept study," in *UV, X-Ray, and Gamma-Ray Space Instrumentation for Astronomy XIX* (International Society for Optics and Photonics, 2015).

[21]W. B. Doriese, K. M. Morgan, D. A. Bennett, E. V. Denison, C. P. Fitzgerald, J. W. Fowler, J. D. Gard, J. P. Hays-Wehle, G. C. Hilton, and K. D. Irwin, "Developments in time-division multiplexing of x-ray transition-edge sensors," J. Low Temp. Phys. **184**(1-2), 389–395 (2016).

[22]P. A. de Korte, J. Beyer, S. Deiker, G. C. Hilton, K. D. Irwin, M. MacIntosh, S. W. Nam, C. D. Reintsema, L. R. Vale, and M. E. Huber, "Time-division superconducting quantum interference device multiplexer for transition-edge sensors," Rev. Sci. Instrum. **74**(8), 3807–3815 (2003).

[23]J. Yoon, J. Clarke, J. Gildemeister, A. T. Lee, M. Myers, P. Richards, and J. Skidmore, "Single superconducting quantum interference device multiplexer for arrays of low-temperature sensors," Appl. Phys. Lett. **78**(3), 371–373 (2001).

[24]L. Gottardi, J. van de Kuur, S. Bandler, M. Bruijn, P. de Korte, J. Gao, R. den Hartog, R. Hijmering, H. Hoevers, and P. Koshropanah, "AC read-out circuits for single pixel characterization of TES microcalorimeters and bolometers," IEEE Trans. Appl. Supercond. **21**(3), 272–275 (2011).

[25]J. Mates, G. C. Hilton, K. D. Irwin, L. R. Vale, and K. W. Lehnert, "Demonstration of a multiplexer of dissipationless superconducting quantum interference devices," Appl. Phys. Lett. **92**(2), 023514 (2008).

[26]W. Yoon, J. Adams, S. Bandler, D. Becker, D. Bennett, J. Chervenak, A. Datesman, M. Eckart, F. Finkbeiner, and J. Fowler, "Toward large field-of-view high-resolution x-ray imaging spectrometers: Microwave multiplexed readout of 28 TES microcalorimeters," J. Low Temp. Phys. **193**(3-4), 258–266 (2018).

[27]G. Stiehl, W. B. Doriese, J. Fowler, G. Hilton, K. Irwin, C. Reintsema, D. Schmidt, D. Swetz, J. Ullom, and L. Vale, "Code-division multiplexing for x-ray microcalorimeters," Appl. Phys. Lett. **100**(7), 072601 (2012).

[28]M. D. Niemack, J. Beyer, H. Cho, W. Doriese, G. Hilton, K. Irwin, C. D. Reintsema, D. R. Schmidt, J. N. Ullom, and L. R. Vale, "Code-division SQUID multiplexing," Appl. Phys. Lett. **96**(16), 163509 (2010).

[29]K. D. Irwin, H.-M. Cho, W. B. Doriese, J. W. Fowler, G. C. Hilton, M. D. Niemack, C. D. Reintsema, D. R. Schmidt, J. N. Ullom, and L. R. Vale, "Advanced code-division multiplexers for superconducting detector arrays," J. Low Temp. Phys. **167**(5-6), 588–594 (2012).

[30]K. M. Morgan, B. K. Alpert, D. A. Bennett, E. Denison, W. Doriese, J. Fowler, J. Gard, G. Hilton, K. Irwin, and Y. Joe, "Code-division-multiplexed readout of large arrays of TES microcalorimeters," Appl. Phys. Lett. **109**(11), 112604 (2016).

[31]C. Titus, S. Chaudhuri, H.-M. Cho, C. Dawson, W. Doriese, J. Fowler, G. Hilton, K. Irwin, S. Kuenstner, and D. Li, "Error-correcting codes for code-division multiplexed TES detectors," J. Low Temp. Phys. **193**(3-4), 556–561 (2018).

[32]W. B. Doriese, P. Abbamonte, B. K. Alpert, D. Bennett, E. Denison, Y. Fang, D. Fischer, C. Fitzgerald, J. Fowler, and J. Gard, "A practical superconducting-microcalorimeter X-ray spectrometer for beamline and laboratory science," Rev. Sci. Instrum. **88**(5), 053108 (2017).

[33]J. Beyer and D. Drung, "A SQUID multiplexer with superconducting-to-normalconducting switches," Supercond. Sci. Technol. **21**(10), 105022 (2008).

[34]A. Szymkowiak, R. Kelley, S. Moseley, and C. Stahle, "Signal processing for microcalorimeters," J. Low Temp. Phys. **93**(3-4), 281–285 (1993).

[35]D. J. Fixsen, S. H. Moseley, B. Cabrera, and E. Figueroa-Feliciano, "Pulse estimation in nonlinear detectors with nonstationary noise," Nucl. Instrum. Methods Phys. Res., Sect. A **520**(1), 555–558 (2004).